Tuning phonon energies in lanthanide-doped potassium lead halide nanocrystals for enhanced nonlinearity and upconversion

Zhuolei Zhang[1,2,#], Artiom Skripka[2,3,#], Jakob C. Dahl[2,4], Chaochao Dun,[2] Jeffrey J. Urban,[2] Daniel Jaque[3], P. James Schuck[5] & Bruce E. Cohen[2,6], Emory M. Chan[2,]*

[1]School of Chemistry and Chemical Engineering, Huazhong University of Science and Technology, 1037 Luoyu Load, Wuhan, 430074 China
[2]The Molecular Foundry, Lawrence Berkeley National Laboratory, Berkeley, California 94720, United States
[3]Nanomaterials for Bioimaging Group, Departamento de Física de Materiales, Facultad de Ciencias, Universidad Autónoma de Madrid, Madrid, 28049, Spain
[4]Department of Chemistry, University of California at Berkeley, Berkeley, California 94720, United States
[5]Department of Mechanical Engineering, Columbia University, New York, New York 10027, United States
[6]Division of Molecular Biophysics & Integrated Bioimaging, Lawrence Berkeley National Laboratory, Berkeley, California 94720, United States

*Corresponding author: emchan@lbl.gov
#These authors have contributed equally

Abstract

Optical applications of lanthanide-doped nanoparticles such as sub-diffraction imaging, photodynamic therapy, and quantum cutting require materials with low phonon energies to minimize nonradiative relaxation and facilitate nonlinear processes such as photon upconversion. Heavy halide hosts offer low phonon energies, but controlled synthesis of stable, doped colloidal nanocrystals has proven challenging. Here, we synthesize low-phonon-energy, KPb_2X_5 (X = Cl, Br) nanoparticles with control of diameter (from 9 to 150 nm), and we demonstrate the ability to tune nanocrystal phonon energies as low as 128 cm^{-1} by careful selection and mixing of halide precursors. These nanoparticles are moisture resistant over 12 weeks and can be efficiently doped with lighter lanthanides. The low phonon energies of KPb_2X_5 nanoparticles promote upconversion emission from lanthanide excited states often quenched by multiphonon relaxation and enable highly nonlinear, avalanche-like emission from $KPb_2Cl_5:Nd^{3+}$ nanoparticles. The realization of nanoparticles with tunable, ultra-low phonon energies provides an approach for discovering nanomaterials with phonon-dependent properties precisely engineered for applications in nanoscale imaging, sensing, and energy conversion.

Manuscript

Inorganic nanocrystals embedded with lanthanide (Ln^{3+}) ions can generate photostable luminescence that drives applications in near-infrared microscopy,[1] sub-diffraction imaging,[2,3] lasing,[4] therapeutics,[5] sensing,[6,7] optogenetics,[8] and quantum cutting.[9,10] The optical performance of these doped materials is strongly influenced by the maximum phonon energy ($\hbar\omega_{max}$) of the nanocrystal host matrix. At moderate and high $\hbar\omega_{max,}$ luminescence is quenched as Ln^{3+} excited states nonradiatively relax via phonon emission, and emission lines are modulated further *via* phonon-assisted energy transfer (PAET). Precise methods for tuning phonon energies would be valuable for manipulating the complex photophysical networks in Ln^{3+}-based nanocrystals[11] and for improving efficiencies of nonlinear optical processes such as upconversion, downconversion,[9,10] and photon avalanching.[12]

To generate upconverted luminescence, Ln^{3+} ions are frequently doped or alloyed into fluoride matrices such as β-$NaYF_4$ to leverage their low $\hbar\omega_{max}$ values (300-500 cm^{-1})[13–16] relative to alternate hosts like oxides (500-600 cm^{-1}), oxysulfides (~520 cm^{-1}), vanadates (~890 cm^{-1}), and garnets (900-1400 cm^{-1}).[17] Low phonon energies discourage multi-phonon relaxation (MPR) because MPR rates decrease exponentially as a greater number of phonons ($\Delta E/\hbar\omega_{max}$) are needed to bridge the energy gap ΔE between adjacent Ln^{3+} states (**Figure 1A**). However, MPR is still prevalent in fluoride nanoparticles (NPs), lowering their quantum yields[18] and limiting applications.

Host matrices based on chlorides, bromides, and iodides exhibit lower phonon energies (120-260 cm^{-1})[19,20] than corresponding fluorides, but synthesis of these halides as doped nanocrystals remains challenging. In addition, many, like $LaCl_3$ ($\hbar\omega_{max} \approx 250$ cm^{-1}),[21] are hygroscopic and decompose in ambient conditions, limiting their development and utility. Bulk KPb_2Cl_5 and KPb_2Br_5 crystals are reportedly more moisture-tolerant than other halides and have bandgaps (3.77 and 3.46 eV, respectively)[22,23] sufficiently wide to be transparent to visible luminescence. While bulk and microscale (>200 nm)[24] crystals of KPb_2Cl_5 have been reported, robust methods for size-controlled synthesis and doping of their NPs analogues are needed, in addition to characterization of their luminescence, stability, and technological applicability. Here, we describe colloidal synthesis of Ln^{3+}-doped nanocrystals with ultra-low phonon energies using KPb_2X_5 (X = Cl, Br) host matrices (**Figure 1A**), and characterize their luminescence and environmental stability. We demonstrate that KPb_2X_5 NP phonon energies can be tuned readily through alloying of their halide ions, and that these perovskite-like nanomaterials are stable under high humidity. The ultra-low $\hbar\omega_{max}$ of these NPs promote upconversion luminescence from Ln^{3+} excited states typically quenched in conventional matrices with higher $\hbar\omega_{max}$ and give rise to steeply nonlinear luminescence in Nd^{3+}-doped KPb_2Cl_5.

To synthesize KPb_2X_5 NPs, we rapidly injected myristoyl halide precursors into 100-310 °C solutions of $Pb(OAc)_4$, K_2CO_3, oleylamine (OM), oleic acid (OA), and octadecene (ODE) (see full synthetic protocols in Supporting Information). Acyl halides react readily with nucleophiles such as OM and oleate ions to release hydrohalic acids (HX) that can react with metal precursors to nucleate and grow KPb_2X_5 NPs.[25] We selected myristoyl halides as precursors due to their high boiling points (~250 °C), which allows for higher reaction temperatures that promote crystallinity and size control of NPs via temporally distinct nucleation.

High-resolution transmission electron microscopy (HRTEM) of KPb_2Cl_5 NPs (**Figure S1**) shows 2.70 Å lattice spacings corresponding to the (311) crystal plane of monoclinic KPb_2Cl_5 with P21/c space group, matching measured and reference (PDF# 01-073-4316) powder X-ray diffraction (XRD) patterns (**Figure 1B**).[24]

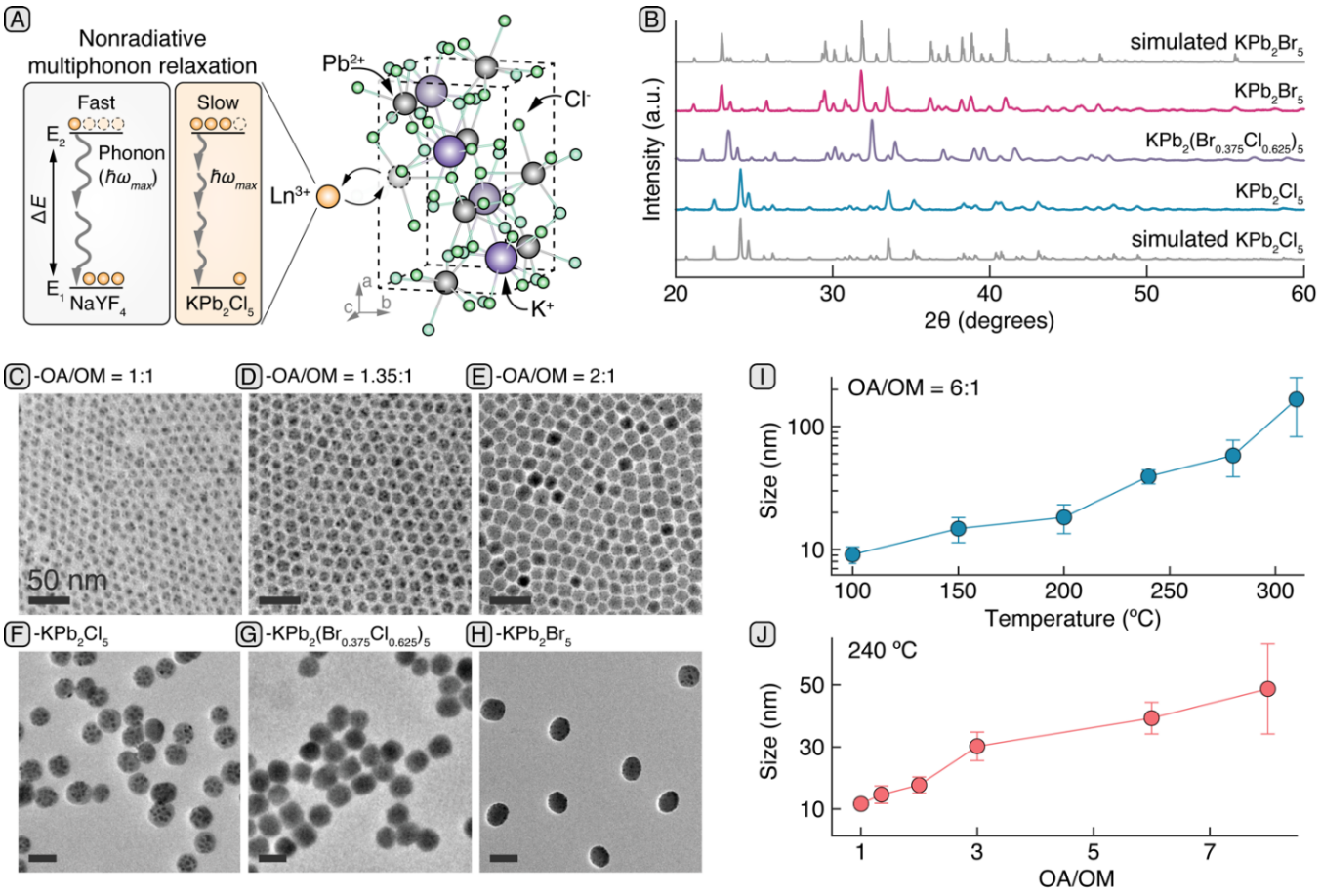

Figure 1. (A) Monoclinic KPb_2Cl_5 lattice and the impact of its low phonon energy ($\hbar\omega_{max}$) on the multi-phonon relaxation (wavy arrows) of Ln^{3+} excited states (E1/E2, populations represented by numbers of circles). (B) XRD patterns of KPb_2Cl_5, $KPb_2(Br_xCl_{1-x})_5$, and KPb_2Br_5 NPs synthesized with 6:1 OA/OM. (C-E) TEM of KPb_2Cl_5 NPs synthesized by tuning OA/OM. (F-H) TEM of KPb_2Cl_5, $KPb_2(Br_xCl_{1-x})_5$, and KPb_2Br_5 NPs synthesized with 6:1 OA/OM. Scale bars in C-H are 50 nm. (I) Diameter vs reaction temperature for KPb_2Cl_5 NPs synthesized with 6:1 OA/OM. (J) Diameter vs OA/OM at 240 °C. Error bars in (I,J) represent ±1 standard deviation in size distribution.

Reaction temperature and OA/OM ratio can each be varied to tune NP size (**Figure 1C-E**, **S2-4**) while maintaining reasonable polydispersity. Varying reaction temperature from 100 to 310 °C produces KPb_2Cl_5 NPs with diameters ranging from 8.9 to 155.0 nm at 6:1 OA/OM (**Figure 1I**). Meanwhile, varying OA/OM from 1:1 to 8:1 fine-tunes diameters from 11.9 to 49.7 nm (240 °C, **Figure 1J**). NP size distributions range from 7 to 50%, (**Figure S3-4**), with the narrowest distributions at low OA/OM and temperature. Increasing OA/OM may increase size and polydispersity by promoting protonation of OM by OA and their condensation into N-oleyloleamide.[26] These reactions can deactivate OM as a nucleophile for acyl halide decomposition, suppressing nucleation.[26,27] OA may also increase NP size by increasing the solubility of metal salts, decreasing nucleation and nuclei growth rates[28] while promoting Ostwald ripening (see Supporting Information).[29]

To determine if this synthetic scheme could produce metal halide nanocrystals with even lower and more tunable phonon energies, we combined appropriate ratios of chloride and bromide precursors to synthesize KPb_2Br_5 and mixed-halide $KPb_2(Br_xCl_{1-x})_5$ NPs (**Figure 1F-H**). Under the same reaction conditions (240 °C and 6:1 OA/OM), KPb_2Cl_5, $KPb_2(Br_{0.375}Cl_{0.625})_5$, and KPb_2Br_5 NPs were synthesized with similar sizes (~40 nm, **Figure S5**). XRD patterns of KPb_2Cl_5, $KPb_2(Br_{0.375}Cl_{0.625})_5$, and KPb_2Br_5 NPs (**Figure 1B**) show pure monoclinic phases, and the single [211] peak of $KPb_2(Br_{0.375}Cl_{0.625})$ ($2\theta = 23.39°$) is positioned between the peaks of pure KPb_2Cl_5 (24.14°) and KPb_2Br_5 (22.94°), corroborating the 5:3 Br:Cl atomic ratio measured by energy-dispersive X-ray spectroscopy (EDS, **Figure S6**) and confirming their successful alloying. Amplitude-averaged phonon energies, extracted from Raman spectra (**Figure 2A**), were 152, 136, and 128 cm^{-1} for undoped KPb_2Cl_5, $KPb_2(Br_{0.375}Cl_{0.625})_5$ and KPb_2Br_5 NPs, respectively. These phonon energies are consistent with those measured for bulk crystals and decrease with the increasing mass of

the halide ion.[19] Notably, KPb_2Cl_5 nanocrystal phonon energies are 2-fold smaller than the ~309 cm^{-1} average phonon energy of β-$NaYF_4$ NPs (**Figure 2A**) most commonly used in Ln^{3+}-based photon upconversion.

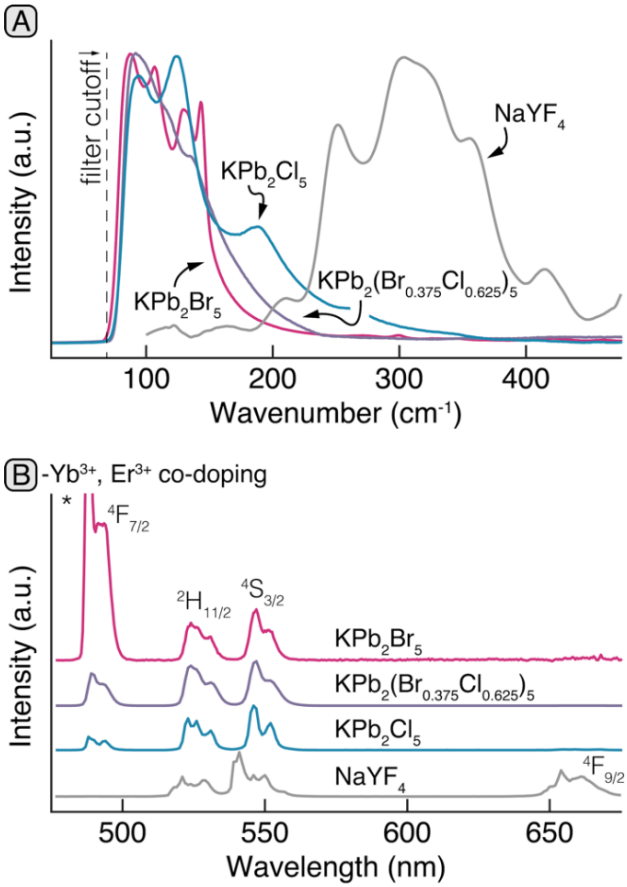

Figure 2. (A) Raman spectra of undoped KPb_2Cl_5, $KPb_2(Br_{0.375}Cl_{0.625})_5$, KPb_2Br_5, and $NaYF_4$ NPs. (B) Upconverted emission spectra of Yb^{3+}, Er^{3+}-codoped KPb_2X_5 and $NaYF_4$ NPs under 980 nm excitation (101 W/cm²). Peaks are labeled by radiative state. *Second order laser artifact.

We further investigated if KPb_2X_5 nanocrystals could host Ln^{3+} ions, and how lower phonon energies influence their luminescence, by incorporating Yb^{3+} and Er^{3+} into reaction solutions. To confirm doping, we measured the elemental compositions of the resulting KPb_2X_5 NPs using EDS (**Figure S8-9**), X-ray photoelectron spectroscopy (**Figure S10**) and inductively coupled plasma optical emission spectroscopy (ICP-OES, **Table S1-2**). Upconversion luminescence spectra of dried KPb_2X_5:Yb^{3+}, Er^{3+} NPs were measured at ambient conditions under 980 nm excitation and examined for differences with canonical $NaYF_4$:Yb^{3+}, Er^{3+} UCNPs. Compared to their $NaYF_4$ counterparts, KPb_2Cl_5: 2.9% Yb^{3+}, 0.6% Er^{3+} NPs show significantly stronger 525 nm emission (Er^{3+}:$^2H_{11/2}$→$^4I_{15/2}$) with respect to their 545 nm ($^4S_{3/2}$→$^4I_{15/2}$) band, approaching a 1:1 ratio. In $NaYF_4$, the Er^{3+}:$^2H_{11/2}$ and $^4S_{3/2}$ manifolds are assumed to be thermally equilibrated since the small, ~700 cm^{-1} energy gap between them is readily bridged by 2 phonons. The enhanced population of the $^2H_{11/2}$ level in KPb_2Cl_5, suggests a dramatic reduction in MPR rate owing to the 2-fold lower $\hbar\omega_{max}$. The NPs also exhibit significantly diminished 660 nm emission (Er^{3+}:$^4F_{9/2}$ → $^4I_{15/2}$) relative to green emission peaks and a prominent emission band around 490 nm ($^4F_{7/2}$ → $^4I_{15/2}$) (**Figure 2B**, **Figure S11-12**). This 490 nm band is typically absent in $NaYF_4$:Yb^{3+},Er^{3+} UCNPs; its intensity is enhanced as $\hbar\omega_{max}$ of the host decreases [compare $KPb_2(Br_{0.375}Cl_{0.625})_5$ and KPb_2Br_5 in **Figure 2B**], providing additional evidence for reduced MPR. To understand the origins of these spectral differences, we used rate equation models (see Supporting Information) to show that 660 nm emission from KPb_2Cl_5:Yb^{3+},Er^{3+} is suppressed due to reduced rates of phonon-assisted transitions that populate the $^4F_{9/2}$ manifold, e.g., MPR from the Er^{3+}:$^4S_{3/2}$ manifold (**Figure S23A**) and cross-relaxation involving the MPR-populated Er^{3+}:$^4I_{13/2}$ manifold (**Figure S23B**).[16,30] In contrast, emission at 490 and 525 nm is enhanced due to reduced MPR from corresponding Er^{3+}:$^4F_{7/2}$ and $^2H_{11/2}$ radiative states (**Figure S23C**). For a complete mechanistic

discussion, see Supporting Information Section S6. We note that KPb_2X_5 NPs are not always brighter, and often dimmer, than their $NaYF_4$ analogues. These comparisons highlight the fact that low-phonon-energy hosts alone may not necessarily improve upconversion intensities, since MPR or PAET is often required to populate states critical to luminescence pathways. Still, the ability to manipulate MPR and PAET rates by tuning host phonon energies provides a method to modulate luminescence from Ln^{3+}-doped NPs and promote emission from excited states normally quenched by MPR, as shown in unconventional upconversion and downshifting spectra of KPb_2Cl_5 NPs doped with Ho^{3+}, Pr^{3+}, Nd^{3+}, Dy^{3+}, and Tm^{3+} (**Figure S14**).

Considering the hygroscopicity and instability of other low-phonon-energy materials, we evaluated the chemical- and photo-stability of the KPb_2Cl_5:Yb^{3+},Er^{3+} NPs under ambient conditions at relative humidities (RH) of 65 and 100%. Films of KPb_2Cl_5 NPs are chemically stable over the course of three months under 65% RH, as demonstrated by the invariance of XRD patterns and upconversion emission intensity (**Figure 3A** and inset). Even at 100% RH, emission spectra (**Figure 3B**) and XRD patterns (**Figure S15**) do not show notable changes after 12 h. KPb_2Cl_5:Yb^{3+},Er^{3+} NPs are also photostable under continuous 980 nm laser irradiation (35 W/cm^2) for 15 h (**Figure S16**), similar to $NaYF_4$ UCNPs. However, immersing powder samples in water causes decomposition of KPb_2Cl_5 NPs (**Figure S17-18**), indicating that additional surface passivation is necessary for aqueous applications.

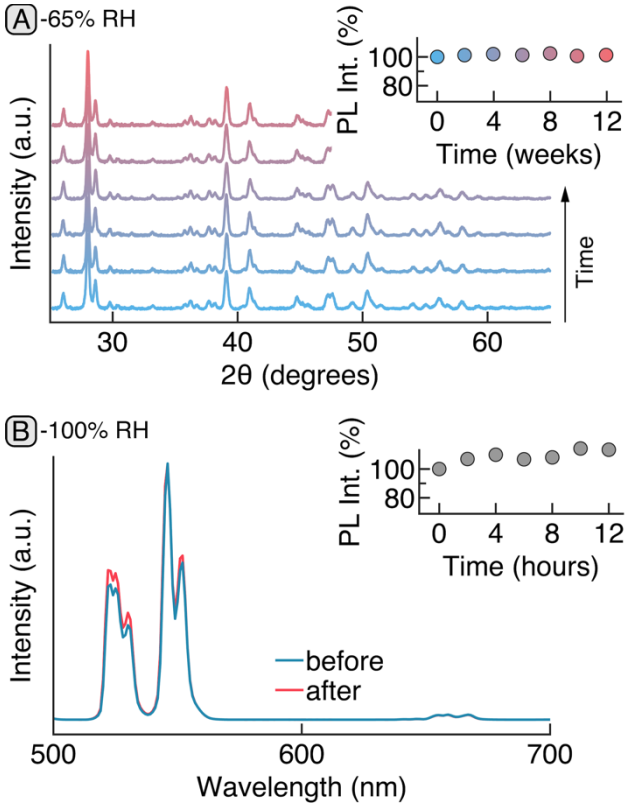

Figure 3. Stability of KPb_2Cl_5:Yb^{3+}, Er^{3+} NPs exposed to (A) 65% RH over 12 weeks, measured by XRD, and to (B) 100% RH over 12 hours, investigated with in situ upconverted luminescence. Insets show temporal evolution of upconversion intensity. XRD pattern colors in (A) indicate exposure times shown in inset.

ICP-OES of Er^{3+}/Yb^{3+} doping into KPb_2X_5 NPs reveals that these heavy Ln^{3+} ions are not efficiently incorporated, regardless of reaction stoichiometry (**Table S1-2**), likely due to differences in charge and ionic radii between Ln^{3+} and Pb^{2+} ions.[31–34] Because the larger radii of lighter Ln^{3+} ions have smaller mismatch with the Pb^{2+}-based matrix, we doped KPb_2Cl_5 NPs with Nd^{3+} ions, commonly used to sensitize 800 nm excitation. ICP-OES shows that KPb_2Cl_5 NPs can be doped with Nd^{3+} ions, with the actual Nd^{3+} composition measured to be 36% of nominal inputs (**Figure 4A, Table S3**). Under 800 nm excitation at ambient conditions, KPb_2Cl_5:0.4% Nd^{3+} NPs demonstrate downshifted NIR emission (883, 1062, 1340 nm) and visible upconversion to 533, 595, and 660 nm (**Figure 4B, Figure S19**), which is notable since upconversion in Nd^{3+}-co-doped $NaYF_4$ has only been observed at >10^6 W/cm^2 excitation in single UCNPs.[35] The ability to control Nd^{3+} doping in KPb_2Cl_5 was also confirmed by the monotonic decrease of the $^4F_{3/2}$

excited-state lifetime (**Figure 4B** inset, **Figure S19**); this quenching is associated with cross-relaxation between Nd^{3+} ions at high concentrations. The $^4F_{3/2}$ lifetime in KPb_2Cl_5:4.1% Nd^{3+} NPs (220 µs) is greater than that of core/shell $NaGdF_4$:5%Nd^{3+}@$NaGdF_4$ NPs (136 µs),[36] and is the result of reduced MPR in KPb_2Cl_5.

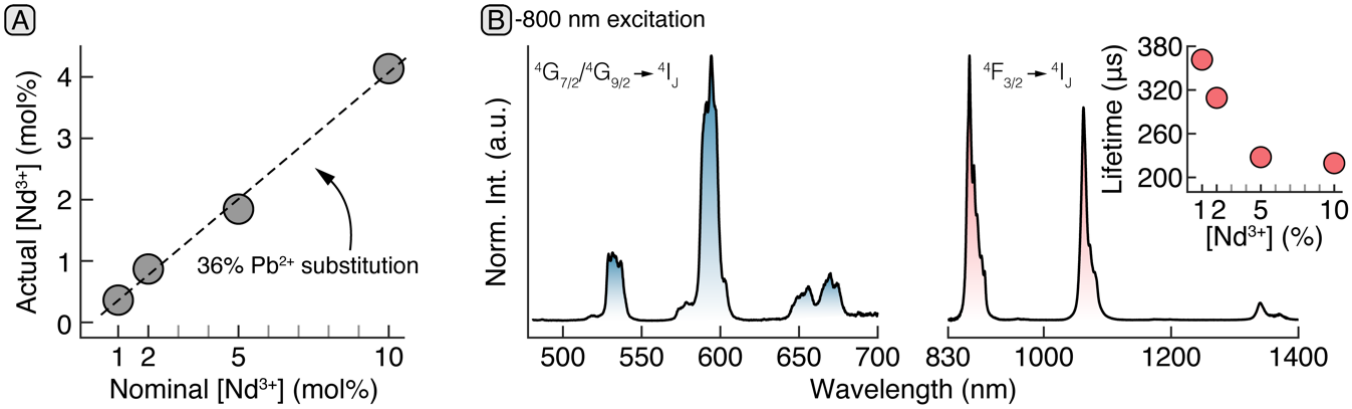

Figure 4. (A) Actual versus nominal [Nd^{3+}] incorporation in KPb_2Cl_5:Nd^{3+} NPs, measured by ICP-OES. (B) Upconverted (*left*) and downshifted (*right*) luminescence spectra of KPb_2Cl_5:0.4% Nd^{3+} NPs under 800 nm (14 W/cm^2) excitation. Inset: $^4F_{3/2}$ excited state lifetimes vs nominal [Nd^{3+}].

The low phonon energy of KPb_2Cl_5 allows us to observe highly nonlinear upconversion emission at visible and NIR wavelengths from heavily doped KPb_2Cl_5:16% Nd^{3+} NPs excited at 1064 nm at room temperature (**Figure 5A**). As the excitation power density (P) is increased above a threshold of ~10 kW/cm^2, the luminescence intensities (I) of major emission lines increase nonlinearly (**Figure 5B**) with power dependence s reaching 9 and 12, at 595 nm and 810 nm, respectively (where $I \propto P^s$). We ascribe this steep power dependence to an energy looping mechanism[37] that nonlinearly amplifies Nd^{3+} excited state populations through repeated cycles of excited state absorption and cross-relaxation (**Figure S24**). Energy looping and its extreme form, photon avalanching (PA),[2] have been predicted in $NaYF_4$:Nd^{3+} NPs but not observed experimentally.[38] KPb_2Cl_5:16% Nd^{3+} NPs meet some (but not all) criteria for PA, including threshold-like behavior (**Figure 5B**) and luminescence rise times that lengthen significantly, to ~70 ms, near avalanching thresholds (**Figure S21**). Such steep nonlinearities suggest that these Nd^{3+}-doped, low-phonon-energy NPs may be useful as probes for sub-diffraction confocal imaging, since the nonlinear Abbe resolution $\delta = \lambda/(2\,NA\,\sqrt{s})$ is 100 nm for s = 12 at 1064 nm pump wavelength (λ) and 1.4 numerical aperture (NA).

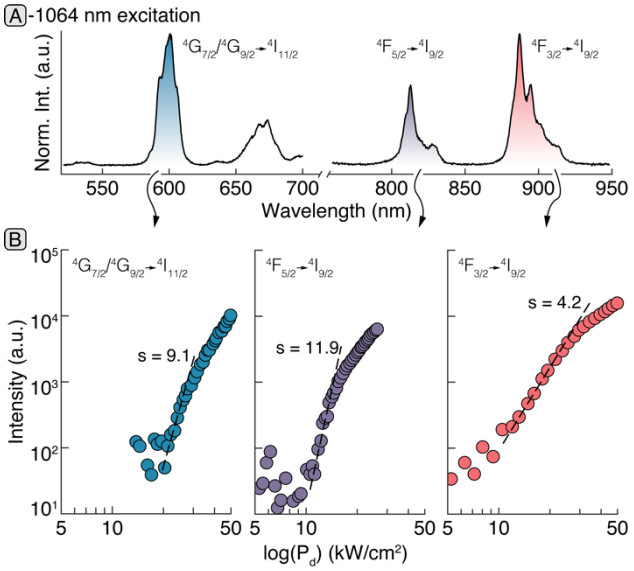

Figure 5. (A) Visible and NIR upconversion spectrum of KPb_2Cl_5: 16%Nd^{3+} NPs under 1064 nm excitation. (B) Emission intensity vs excitation power of the most intense Nd^{3+} upconversion bands, showing steeply nonlinear upconversion. Dashed lines are linear fits at maximum slope s for each curve.

We have demonstrated the size-controlled synthesis of low-phonon-energy, Ln^{3+}-doped KPb_2X_5 NPs stable towards humidity. The ultra-low phonon energies of these materials (120-160 cm^{-1}) enabled discovery of highly nonlinear, avalanche-like Nd^{3+} emission and Ln^{3+} emission lines not observed in fluoride UCNPs, facilitating multicolor widefield and sub-diffraction imaging. Finally, intensities of low-phonon-energy NPs suggest that Ln^{3+} luminescence is maximized not at the lowest phonon energies, but at phonon energies that simultaneously minimize deleterious MPR while maintaining critical phonon-assisted pathways. The mixed-halide alloying approach demonstrated here will facilitate such optimization and will be valuable for manipulating complex photophysical networks in Ln^{3+}-based nanomaterials and other phonon-dependent systems.

Author Contributions

#These authors contributed equally. All authors have given approval to the final manuscript.

Notes

The authors declare no competing financial interest.

Acknowledgments

This study is based on work supported by the Defense Advanced Research Projects Agency (DARPA) under Contract No. HR001118C0036. Any opinions, findings and conclusions or recommendations expressed in this material are those of the authors and do not necessarily reflect the views of DARPA. Work at the Molecular Foundry was supported by the Office of Science, Office of Basic Energy Sciences, of the U.S. Department of Energy under Contract No. DE-AC02-05CH11231. Work at Universidad Autónoma de Madrid was financed by the Spanish Ministerio de Innovación y Ciencias under project NANONERV PID2019-106211RB-100, with additional funding provided by COST action CA17140. Work at the Huazhong University of Science and Technology was supported by the Start-up Funding of HUST. A.S. acknowledges support from the European Union's Horizon 2020 research and innovation program under the Marie Skłodowska-Curie grant agreement No. 895809 (MONOCLE).

References:

(1) Wen, S.; Zhou, J.; Zheng, K.; Bednarkiewicz, A.; Liu, X.; Jin, D. Advances in Highly Doped Upconversion Nanoparticles. *Nat. Commun.* **2018**, *9* (1), 2415.

(2) Lee, C.; Xu, E. Z.; Liu, Y.; Teitelboim, A.; Yao, K.; Fernandez-Bravo, A.; Kotulska, A. M.; Nam, S. H.; Suh, Y. D.; Bednarkiewicz, A.; Cohen, B. E.; Chan, E. M.; Schuck, P. J. Giant Nonlinear Optical Responses from Photon-Avalanching Nanoparticles. *Nature* **2021**, *589* (7841), 230–235.

(3) Liu, Y.; Lu, Y.; Yang, X.; Zheng, X.; Wen, S.; Wang, F.; Vidal, X.; Zhao, J.; Liu, D.; Zhou, Z.; Ma, C.; Zhou, J.; Piper, J. A.; Xi, P.; Jin, D. Amplified Stimulated Emission in Upconversion Nanoparticles for Super-Resolution Nanoscopy. *Nature* **2017**, *543* (7644), 229–233.

(4) Liu, Y.; Teitelboim, A.; Fernandez-Bravo, A.; Yao, K.; Altoe, M. V. P.; Aloni, S.; Zhang, C.; Cohen, B. E.; Schuck, P. J.; Chan, E. M. Controlled Assembly of Upconverting Nanoparticles for Low-Threshold Microlasers and Their Imaging in Scattering Media. *ACS Nano* **2020**, *14* (2), 1508–1519.

(5) Skripka, A.; Karabanovas, V.; Jarockyte, G.; Marin, R.; Tam, V.; Cerruti, M.; Rotomskis, R.; Vetrone, F. Decoupling Theranostics with Rare Earth Doped Nanoparticles. *Adv. Funct. Mater.* **2019**, *29* (12), 1807105.

(6) Lay, A.; Wang, D. S.; Wisser, M. D.; Mehlenbacher, R. D.; Lin, Y.; Goodman, M. B.; Mao, W. L.; Dionne, J. A. Upconverting Nanoparticles as Optical Sensors of Nano- to Micro-Newton Forces. *Nano Lett.* **2017**, *17* (7), 4172–4177.

(7) Liu, X.; Skripka, A.; Lai, Y.; Jiang, C.; Liu, J.; Vetrone, F.; Liang, J. Fast Wide-Field Upconversion Luminescence Lifetime Thermometry Enabled by Single-Shot Compressed Ultrahigh-Speed Imaging. *Nat. Commun.* **2021**, *12* (1), 6401.

(8) Wu, X.; Zhang, Y.; Takle, K.; Bilsel, O.; Li, Z.; Lee, H.; Zhang, Z.; Li, D.; Fan, W.; Duan, C.; Chan, E. M.; Lois, C.; Xiang, Y.; Han, G. Dye-Sensitized Core/Active Shell Upconversion Nanoparticles for Optogenetics and Bioimaging Applications. *ACS Nano* **2016**, *10* (1), 1060–1066.

(9) Wegh René T.; Donker Harry; Oskam Koenraad D.; Meijerink Andries. Visible Quantum Cutting in LiGdF4:Eu3+ Through Downconversion. *Science* **1999**, *283* (5402), 663–666.

(10) Shao, W.; Lim, C.-K.; Li, Q.; Swihart, M. T.; Prasad, P. N. Dramatic Enhancement of Quantum Cutting in Lanthanide-Doped Nanocrystals Photosensitized with an Aggregation-Induced Enhanced Emission Dye. *Nano Lett.* **2018**, *18* (8), 4922–4926.

(11) Teitelboim, A.; Tian, B.; Garfield, D. J.; Fernandez-Bravo, A.; Gotlin, A. C.; Schuck, P. J.; Cohen, B. E.; Chan, E. M. Energy Transfer Networks within Upconverting Nanoparticles Are Complex Systems with Collective, Robust, and History-Dependent Dynamics. *J. Phys. Chem. C* **2019**, *123* (4), 2678–2689.

(12) Zheng, B.; Fan, J.; Chen, B.; Qin, X.; Wang, J.; Wang, F.; Deng, R.; Liu, X. Rare-Earth Doping in Nanostructured Inorganic Materials. *Chem. Rev.* **2022**, *122* (6), 5519–5603.

(13) Suyver, J. F.; Grimm, J.; van Veen, M. K.; Biner, D.; Krämer, K. W.; Güdel, H. U. Upconversion Spectroscopy and Properties of NaYF4 Doped with Er3+, Tm3+ and/or Yb3+. *J. Lumin.* **2006**, *117* (1), 1–12.

(14) Wang, F.; Liu, X. Upconversion Multicolor Fine-Tuning: Visible to Near-Infrared Emission from Lanthanide-Doped NaYF4 Nanoparticles. *J. Am. Chem. Soc.* **2008**, *130* (17), 5642–5643.

(15) Gargas, D. J.; Chan, E. M.; Ostrowski, A. D.; Aloni, S.; Altoe, M. V. P.; Barnard, E. S.; Sanii, B.; Urban, J. J.; Milliron, D. J.; Cohen, B. E.; Schuck, P. J. Engineering Bright Sub-10-Nm Upconverting Nanocrystals for Single-Molecule Imaging. *Nat. Nanotechnol.* **2014**, *9* (4), 300–305.

(16) Tian, B.; Fernandez-Bravo, A.; Najafiaghdam, H.; Torquato, N. A.; Altoe, M. V. P.; Teitelboim, A.; Tajon, C. A.; Tian, Y.; Borys, N. J.; Barnard, E. S.; Anwar, M.; Chan, E. M.; Schuck, P. J.; Cohen, B. E. Low Irradiance Multiphoton Imaging with Alloyed Lanthanide Nanocrystals. *Nat. Commun.* **2018**, *9* (1), 3082.

(17) Chen, G.; Qiu, H.; Prasad, P. N.; Chen, X. Upconversion Nanoparticles: Design, Nanochemistry, and Applications in Theranostics. *Chem. Rev.* **2014**, *114* (10), 5161–5214.

(18) Fischer, S.; Bronstein, N. D.; Swabeck, J. K.; Chan, E. M.; Alivisatos, A. P. Precise Tuning of Surface Quenching for Luminescence Enhancement in Core–Shell Lanthanide-Doped Nanocrystals. *Nano Lett.* **2016**, *16* (11), 7241–7247.

(19) Hehlen, M. P.; Krämer, K.; Güdel, H. U.; McFarlane, R. A.; Schwartz, R. N. Upconversion in Er3+-Dimer Systems: Trends within the Series Cs3Er2X9 (X=Cl,Br,I). *Phys. Rev. B* **1994**, *49* (18), 12475–12484.

(20) Shojiya, M.; Takahashi, M.; Kanno, R.; Kawamoto, Y.; Kadono, K. Upconversion Luminescence of Er3+ in CdX2 System Glasses (X=Cl, Br, I). *Appl. Phys. Lett.* **1995**, *67* (17), 2453–2455.

(21) Richman, I.; Satten, R. A.; Wong, E. Y. Lattice Vibrations of LaCl3 and LaBr3 from Vibronic Spectra. *J. Chem. Phys.* **1963**, *39* (7), 1833–1846.

(22) Vu, T. V.; Lavrentyev, A. A.; Gabrelian, B. V.; Vo, D. D.; Tong, H. D.; Denysyuk, N. M.; Isaenko, L. I.;

Tarasova, A. Y.; Khyzhun, O. Y. Theoretical and Experimental Study on the Electronic and Optical Properties of K0.5Rb0.5Pb2Br5: A Promising Laser Host Material. *RSC Adv.* **2020**, *10* (19), 11156–11164.
(23) Hommerich, U.; Uba, S.; Kabir, A.; Trivedi, S. B.; Yang, C.; Brown, E. E. Visible Emission Studies of Melt-Grown Dy-Doped CsPbCl3 and KPb2Cl5 Crystals. *Opt. Mater. Express* **2020**, *10* (8), 2011–2018.
(24) Lim, S.-C.; Lin, H.-P.; Tsai, W.-L.; Lin, H.-W.; Hsu, Y.-T.; Tuan, H.-Y. Binary Halide, Ternary Perovskite-like, and Perovskite-Derivative Nanostructures: Hot Injection Synthesis and Optical and Photocatalytic Properties. *Nanoscale* **2017**, *9* (11), 3747–3751.
(25) Imran, M.; Caligiuri, V.; Wang, M.; Goldoni, L.; Prato, M.; Krahne, R.; De Trizio, L.; Manna, L. Benzoyl Halides as Alternative Precursors for the Colloidal Synthesis of Lead-Based Halide Perovskite Nanocrystals. *J. Am. Chem. Soc.* **2018**, *140* (7), 2656–2664.
(26) Ostrowski, A. D.; Chan, E. M.; Gargas, D. J.; Katz, E. M.; Han, G.; Schuck, P. J.; Milliron, D. J.; Cohen, B. E. Controlled Synthesis and Single-Particle Imaging of Bright, Sub-10 Nm Lanthanide-Doped Upconverting Nanocrystals. *ACS Nano* **2012**, *6* (3), 2686–2692.
(27) Almeida, G.; Goldoni, L.; Akkerman, Q.; Dang, Z.; Khan, A. H.; Marras, S.; Moreels, I.; Manna, L. Role of Acid–Base Equilibria in the Size, Shape, and Phase Control of Cesium Lead Bromide Nanocrystals. *ACS Nano* **2018**, *12* (2), 1704–1711.
(28) Owen, J. S.; Chan, E. M.; Liu, H.; Alivisatos, A. P. Precursor Conversion Kinetics and the Nucleation of Cadmium Selenide Nanocrystals. *J. Am. Chem. Soc.* **2010**, *132* (51), 18206–18213.
(29) Yang, H.; Hamachi, L. S.; Rreza, I.; Wang, W.; Chan, E. M. Design Rules for One-Step Seeded Growth of Nanocrystals: Threading the Needle between Secondary Nucleation and Ripening. *Chem. Mater.* **2019**, *31* (11), 4173–4183.
(30) Chan, E. M.; Han, G.; Goldberg, J. D.; Gargas, D. J.; Ostrowski, A. D.; Schuck, P. J.; Cohen, B. E.; Milliron, D. J. Combinatorial Discovery of Lanthanide-Doped Nanocrystals with Spectrally Pure Upconverted Emission. *Nano Lett.* **2012**, *12* (7), 3839–3845.
(31) Aarts, L.; Jaeqx, S.; van der Ende, B. M.; Meijerink, A. Downconversion for the Er3+, Yb3+ Couple in KPb2Cl5—A Low-Phonon Frequency Host. *J. Lumin.* **2011**, *131* (4), 608–613.
(32) Tkachuk, A. M.; Ivanova, S. É.; Isaenko, L. I.; Yelisseyev, A. P.; Joubert, M.-F.; Guyot, Y.; Payne, S. Spectroscopic Studies of Erbium-Doped Potassium-Lead Double Chloride Crystals KPb2Cl5:Er3+: 1. Optical Spectra and Relaxation of Excited States of the Erbium Ion in Potassium-Lead Double Chloride Crystals. *Opt. Spectrosc.* **2003**, *95* (5), 722–740.
(33) Cascales, C.; Fernández, J.; Balda, R. Investigation of Site-Selective Symmetries of Eu3+ Ions in KPb2Cl5 by Using Optical Spectroscopy. *Opt. Express* **2005**, *13* (6), 2141–2152.
(34) Marin, R.; Jaque, D. Doping Lanthanide Ions in Colloidal Semiconductor Nanocrystals for Brighter Photoluminescence. *Chem. Rev.* **2021**, *121* (3), 1425–1462.
(35) Liao, J.; Jin, D.; Chen, C.; Li, Y.; Zhou, J. Helix Shape Power-Dependent Properties of Single Upconversion Nanoparticles. *J. Phys. Chem. Lett.* **2020**, *11* (8), 2883–2890.
(36) Skripka, A.; Benayas, A.; Brites, C. D. S.; Martín, I. R.; Carlos, L. D.; Vetrone, F. Inert Shell Effect on the Quantum Yield of Neodymium-Doped Near-Infrared Nanoparticles: The Necessary Shield in an Aqueous Dispersion. *Nano Lett.* **2020**, *20* (10), 7648–7654.
(37) Levy, E. S.; Tajon, C. A.; Bischof, T. S.; Iafrati, J.; Fernandez-Bravo, A.; Garfield, D. J.; Chamanzar, M.; Maharbiz, M. M.; Sohal, V. S.; Schuck, P. J.; Cohen, B. E.; Chan, E. M. Energy-Looping Nanoparticles: Harnessing Excited-State Absorption for Deep-Tissue Imaging. *ACS Nano* **2016**, *10* (9), 8423–8433.
(38) Bednarkiewicz, A.; Chan, E. M.; Kotulska, A.; Marciniak, L.; Prorok, K. Photon Avalanche in Lanthanide Doped Nanoparticles for Biomedical Applications: Super-Resolution Imaging. *Nanoscale Horiz.* **2019**, *4* (4), 881–889.